Title
Earthquake slip distribution: A statistical model

Journal
Journal of Geophysical Research-Solid Earth, 110(B5)

ISSN
0148-0227

Author
Kagan, Yan Y

Publication Date
2005-03-01

Peer reviewed

JOURNAL OF GEOPHYSICAL RESEARCH, VOL. 110, XXXX, DOI:10.1029/,

PostScript file created: May 16, 2011

EARTHQUAKE SLIP DISTRIBUTION: A STATISTICAL MODEL

Yan Y. Kagan[1]

[1] Department of Earth and Space Sciences, University of California, Los Angeles, California, USA

Abstract. The purpose of this paper is to interpret slip statistics in a framework of extended earthquake sources. We first discuss the deformation pattern of the Earth's surface from earthquakes and suggest that the continuum versus block motion controversy can be reconciled by the model of a fractal distribution of seismic sources. We consider earthquake slip statistical distributions as they can be inferred from seismic moment-frequency relations and geometrical scaling for earthquakes. Using various assumptions on temporal earthquake occurrence, these distributions are synthesized to evaluate the accuracy of geologic fault slip determinations and to estimate uncertainties in long-term earthquake patterns based on paleoseismic data. Because the seismic moment distribution is a power-law (Pareto), a major part of the total seismic moment is released by major earthquakes, $M \geq 10^{19.5}$ Nm (moment magnitude $m \geq 7$); for these large earthquakes the rupture is confined to the upper brittle layer of the crust. We review the various moment-frequency and earthquake scaling relationships and apply them to infer the slip distribution at area- and site-specific regions. Simulating the seismic moment and strain accumulation process demonstrates that some synthetics can be interpreted as examples of a quasi-periodic sequence. We demonstrate the application of the derived slip statistical relations by analyzing the slip distribution and history of the San Andreas fault at Wrightwood, CA.

INDEX TERMS: Seismology (ESE): 7215 Earthquake parameters; 7230 Seismicity and seismotectonics; 7221 Paleoseismology

KEYWORDS: Seismic moment distribution, Earthquake slip, Spatial earthquake scaling, Fractal earthquake distribution, Power-law (Pareto) distributions of earthquake parameters

1. Introduction

This paper is meant to be the first in a series that will describe statistically deformation of the Earth's surface from earthquakes. When completed the statistical model can be compared with results of detailed GPS [*Jackson et al.*, 1997; *Sagiya*, 2004] and InSAR measurements. This task cannot be undertaken now because needed theoretical tools are still unavailable and observational results are not sufficient for extensive statistical analysis. However, we discuss below (especially in the Discussion section) what statistical methods should be developed and what measurements attempted to enable construction of a complex, comprehensive model.

We have a much more modest aim here: to present a statistical model of slip distributions due to earthquakes. Slip measurements are being carried out at particular points along faults in California [*Sieh et al.*, 1989; *Yeats et al.*, 1997; *Rockwell et al.*, 2000; *Weldon et al.*, 2002; *Rockwell et al.*, 2002; *Scharer et al.*, 2003; *Liu et al.*, 2004] and in other places. Histories of vertical displacements have been investigated in coral reefs [*Natawidjaja et al.*, 2004] and in uplifts of marine/fluvial terraces along many Pacific subduction zones. These observations can be compared to the theoretical derivations of this paper to evaluate the statistical properties of these time series. Here we try to create only the methodological tools for such an exercise; the few applications of the statistical analysis discussed below are meant only as illustrations. A full statistical analysis of these data would need cooperation between several Earth science specialties.

To create the statistical model for earthquake slip distribution, we consider three interrelated problems: earthquake size distribution, scaling of geometric parameters with earthquake size, and the temporal behavior of seismicity, especially in the largest earthquakes. These problems need to be solved to estimate the accumulation and release of strain by earthquakes in plate boundary zones and zones of distributed deformation. Until recently, studies of earthquake statistical distributions presented earthquakes as points in space and time. Even in those cases where the extent of rupture has been investigated, it was done by studying the data for individual earthquakes. Here we combine known earthquake distributions to present a geometrical and statistical picture of deformation at certain points along seismogenic fault.

Most tectonic strain is released by the largest earthquakes [*Brune*, 1968; *Kagan*, 2002a]. There is little uncertainty about the size distribution for small and moderate earthquakes: they follow the Gutenberg-Richter (G-R) relation. A similar conclusion is valid for moderate and large earthquakes distributed over large seismogenic regions [*Utsu*, 1999]. *Kagan* [1999; 2002a,b] and *Bird and Kagan* [2004] argue that earthquake size distribution has a universal b-value. An upper bound or maximum magnitude needs to be introduced for earthquake size distributions [*Kagan*, 2002a,b]. We review several distributions in which this limit is applied and consider its influence on estimating rate of seismic deformation and slip.

Despite extensive investigations and an extended debate (see, for example, *Scholz* [1997; 1998]; *Romanowicz* [1994]; *Abercrombie* [1995]; *Main* [2000]; Romanowicz and Ruff

0148-0227/11/$9.00

[2002]), no consensus exists on scaling relationships between earthquake seismic moment and geometric variables such as the rupture length, width, and average slip. Therefore, we will explore different scaling relations. What are their implications for statistical distributions of slip?

The G-R relation for magnitudes is equivalent to the power-law (Pareto) distribution for the seismic moment [*Utsu*, 1999; *Kagan*, 2002a;b]. This implies that the geometry of earthquake rupture is also controlled by power-law distributions. Depending on the value of the exponent, sums of power-law variables may not converge to any finite value [*Zaliapin et al.*, 2005] or may be highly fluctuating.

If a maximum size in a power-law earthquake size distribution is present, the sum distribution and its random fluctuations strongly differ from that for regular statistical variables, following the Gaussian law which is mostly (explicitly or more often implicitly) used in geophysical practice. For example, *Holt et al.* [2000] found that a sum of earthquake seismic moments for some regions of south-eastern Asia may exceed the tectonic rate by a factor of 3 to 5 and more. This difference cannot be explained by any errors in tectonic rate calculations or seismic moment evaluation. The mismatch is clearly caused by random fluctuations of the power-law distributed variable. This highly random behavior of cumulative seismic moment necessitates a new way to compare seismic and tectonic rates [*Kagan*, 1999; 2002a;b; *Kreemer et al.*, 2003; *Bird and Kagan*, 2004]. Thus, we will discuss statistical properties of accumulated earthquake slip and consider appropriate estimates of statistical error for measuring it.

In studying slip distribution we should proceed from representing a point source to the approach based on extended earthquake rupture. This change requires applying statistical distributions of the rupture length, width and slip to infer the pattern of average slip not only for a region or an area, but also for a specific place on a fault.

The temporal pattern of large earthquakes is key to the distribution of cumulative earthquake slip. Unfortunately, it is still not known whether large events cluster in time, or follow a quasi-periodic pattern. Long-term earthquake hazard estimates are usually based on the Poisson assumption: occurrence of one event is statistically unrelated to occurrence of others. Thus, we need to consider various hypotheses of moment and slip release in time and their impact on slip distribution.

An additional issue needs to be discussed: how earthquake rupture is concentrated in space. Two models are commonly used – tectonic block motion and continuum deformation. The former model envisions a very narrow concentration of ruptures, whereas the latter expects the deformation to be broadly distributed. As we show in Section 2, in reality both points of view are somewhat valid; the spatial fractal framework combines and synthesizes both these hypotheses.

In this paper, first we will discuss the earthquake size distribution (seismic moment-frequency relation) and review the major theoretical relations proposed to approximate observational data (Section 3). Section 4 reviews models for earthquake scaling, or the relationship between the seismic moment and rupture geometry. We obtain statistical expressions for rupture lengths and slip distributions based on scaling and magnitude-frequency relations. Section 5 applies the above relations to earthquake ruptures at specific sites of a fault. Temporal distributions of large earthquakes and slip accumulation at a specific point of a fault are considered in Section 6. We illustrate the obtained results by evaluating statistical properties of slip distribution at Wrightwood, CA on the San Andreas fault. The Discussion section and Conclusion summarize our results. Three appendices contain some technical statistical formulas, and they are included in the electronic supplement.

2. Deformation pattern: Continuum versus block motion

King et al. [1994] ask whether block or continuum deformation should be used to describe patterns of seismicity and deformation in the western United States. A continuous representation is usually used for large seismic regions (e.g., *Holt et al.* [2000]; *Kreemer et al.* [2003]). For smaller, extensively studied regions such as California, earthquake deformation is normally represented as occurring on specific faults [*Wesnousky*, 1986].

Earthquake data are traditionally displayed as epicenter points or focal mechanisms on a map, although the rupture's extent can be estimated from surface rupture traces and aftershock distributions. To analyze strain at the Earth's surface, we need to display earthquake sources as extended ruptures, at least for large earthquakes. To exemplify earthquake data, Fig. 1 in the companion paper [*Kagan et al.*, 2005] shows focal mechanisms for moderate and large earthquakes in southern California from 1850-2003. The diagram suggests that earthquakes are not concentrated on a few faults. The mechanisms of neighboring events may have a very different orientation. Even in a neighborhood of major faults, some focal mechanisms significantly disagree with fault surface traces. This mismatch confirms the idea that major faults do not fully represent the deformation pattern, even in a region with relatively simple and well-studied tectonics. In contrast, measuring deformation on major faults and in their neighborhood indicates that most strain is within confined zones (often narrow enough to trench in paleoseismic investigations). Both findings suggest that block and continuum hypotheses need to be combined in a joint model.

Kagan and Knopoff [1980] and *Kagan* [1991] show that the spatial distribution of epicenters and hypocenters can be described by a fractal, scale-invariant relation with the value of the correlation dimension $\delta \approx 2.2 - 2.3$. These results imply that neither block models (with a finite number of faults) nor continuous models can accurately describe the tectonic deformation pattern.

In this paper we concentrate on studying slip on individual fault segments. Observations (e.g., *Sieh et al.* [1989]; *Weldon et al.* [2002]) and modeling of fractal fault systems [*Kagan*, 1982; *Libicki and Ben-Zion*, 2005] suggest that while faults generally show a complicated fractal branching structure, much tectonic deformation is concentrated in very narrow zones in certain places. These zones can be represented by a planar fault intersecting the Earth's surface, displacing river valleys and other geomorphic features by measurable distances. Such displacements are often used to estimate the average fault slip rate. Given that no statistical description of a fault displacement exists, it is difficult to estimate uncertainties in evaluating the rate, at least those uncertainties arising from random fluctuations. Thus, we will model fault deformation statistically and estimate random errors in tectonic rate calculation quantitatively. As explained in the Introduction, for power-law distributed variables, statistical fluctuations can be very large. To evaluate them, we should know their statistical properties.

3. Seismic moment statistical distribution

We need to find the most appropriate statistical relationship that describes earthquake size distribution. The relation between magnitude and moment-frequency is one of the most studied statistical properties of earthquake occurrence. However, many unresolved controversies remain open in the

properties of earthquake size distribution. We review these below, emphasizing the moment distribution features.

We use the notation M for the scalar seismic moment and m for the moment magnitude [*Hanks*, 1992]:

$$m = \frac{2}{3} \log_{10} M - 6.0 \,, \tag{1}$$

where M is measured in Newton-m (Nm). The magnitude calculated by Equation (1) is used here for illustration and as a proxy for the seismic moment. All pertinent computations are carried out with moment estimates.

3.1. Theoretical distributions

In this subsection we briefly review statistical distributions for approximating the moment-frequency relation. For a more complete discussion see *Kagan* [2002a;b] and *Bird and Kagan* [2004]. The earthquake size distribution is usually described by the G-R magnitude-frequency law

$$\log_{10} N(m) = a - bm \,, \tag{2}$$

where $N(m)$ is the number of earthquakes with magnitude $\geq m$, and $b \approx 1$.

Utsu [1999, his Eq. 5, see also *Aki*, 1965] explains that the G-R law (Equation 2) is equivalent to the exponential statistical distribution (see, e.g., *Evans et al.* [1993]) for magnitudes. For earthquake energy or seismic moment (Equation 2) can be converted to a power-law relation [*Utsu*, 1999, his Eq. 2], or, as this distribution is known in statistics, the Pareto distribution [*Evans et al.* 1993], with the power exponent $\beta = b/1.5$. Because seismographic networks have limited sensitivity, small earthquakes are not completely sampled in earthquake catalogs. Thus, we must introduce a catalog completeness threshold (cutoff) M_t and truncate the distribution from the left:

$$\phi(M) \;=\; \beta \, M_t^{\beta} \, M^{-1-\beta} \qquad \text{for} \quad M_t \leq M < \infty \,. \tag{3}$$

The threshold magnitude varies from about 1.0 for modern local catalogs like that of southern California to about 5.5 for the Harvard CMT catalog [*Ekström et al.*, 2003].

Two types of errors need to be considered in fitting the theoretical earthquake size distribution to data: uncertainty in estimating the β-value and random fluctuations of earthquake numbers. Fig. 1 displays the moment-frequency relation in the southern California area for 1800-1999, using the *Toppozada et al.* [2000] catalog. We approximate the observational curve by the Pareto distribution (3). The displayed 95% confidence limits for β [*Aki*, 1965; *Kagan*, 2002a] are conditioned by the total number of earthquakes observed. To calculate full uncertainty bounds, it is necessary to convolve β-errors with the event number distribution. We make the simplest assumption that this distribution is Poisson. For the number (N) of samples in the Poisson distribution greater than 30, one can use the Gaussian approximation with the variance equal to N. Thus, the total number of events in the subcatalog has the standard error 197 ± 14.0. To make the calculations easy for this illustrative diagram, we extend this approximation down to $N = 1$. For the upper limit, the resulting uncertainties shown by the upper dashed curve in the plot are smaller than the actual Poisson bounds, so our limit is under-estimate of the actual uncertainty spread. For the lower limit, the opposite is true, so that the real lower limit should be between the β (solid) line and the dashed line shown in the plot.

Simple considerations of the finiteness of seismic moment flux or of deformational energy available for an earthquake generation [*Kagan*, 2002a;b] require that the Pareto relation (3) be modified at the large size end of the moment scale. Below we consider four theoretical distributions to describe seismic moment-frequency relations with an upper bound [*Kagan*, 2002a;b]:
(a) the characteristic distribution;
(b) the truncated Pareto distribution;
(c) the modified G-R distribution, and
(d) the gamma distribution.
These distributions have a scale-invariant, power-law segment for small and moderate earthquakes; the right-hand tail of the distributions is controlled by the maximum moment value. Thus, models (a-d) extend the classical G-R law using an upper bound, M_x. We employ the notation M_{xc}, M_{xp}, M_{cm}, M_{cg}, respectively, for the maximum seismic moment of each distribution. In the last two cases the limit at the tail of the distribution is not a 'hard' cutoff as in (a)-(b), but a 'soft' taper. It would be more appropriate to define M_{cm} and M_{cg} as 'corner' moments.

For case (a) the distribution is described by the function $\Phi(M)$,

$$\begin{aligned} \Phi(M) \;&=\; 1 - F(M) \;=\; (M_t/M)^{\beta} \\ &\text{for} \quad M_t \leq M \leq M_{xc}, \quad \text{and} \\ \Phi(M) \;&=\; 0 \qquad \text{for} \quad M > M_{xc} \,, \end{aligned} \tag{4}$$

where $F(M)$ is a cumulative function, M_{xc} is the maximum moment. Equation (4) does not exactly correspond to the characteristic earthquake model as formulated by *Schwartz and Coppersmith* [1984] or by *Wesnousky* [1994]. In their model the characteristic earthquakes release about 87% of the total moment [*Kagan*, 1996]. In case (a) only 33% (for $\beta = 2/3$) of the total is released by the characteristic events [*Kagan*, 2002b]. *Kagan* [1996] criticizes using the characteristic model for seismicity analysis; see also *Wesnousky* [1996], *Rong et al.* [2003], and *Stein and Newman* [2004] for more discussion. We use model (a) here for illustration, as it is more compatible with other distributions (b-d).

Similarly, for (b)

$$\begin{aligned} \Phi(M) \;&=\; \frac{(M_t/M)^{\beta} - (M_t/M_{xp})^{\beta}}{1 - (M_t/M_{xp})^{\beta}} \\ &\text{for} \quad M_t \leq M \leq M_{xp} \,. \end{aligned} \tag{5}$$

For the tapered G-R and gamma distributions the expressions are

$$\begin{aligned} \Phi(M) \;&=\; (M_t/M)^{\beta} \, \exp\left(\tfrac{M_t - M}{M_{cm}}\right) \\ &\text{for} \quad M_t \leq M < \infty, \end{aligned} \tag{6}$$

and

$$\Phi(M) \;=\; C^{-1} (M_t/M)^{\beta} \exp\left(\frac{M_t - M}{M_{cg}}\right)$$
$$\times \left[1 \; - (M/M_{cg})^{\beta} \exp(M/M_{cg}) \; \Gamma(1-\beta, M/M_{cg})\right] \,, \tag{7}$$

where the normalization coefficient C is defined by Eq. (17) in *Kagan* [2002a] (for $M_{cg} >> M_t$ the coefficient $C \approx 1$) and $\Gamma(a,b)$ is the incomplete gamma function [*Abramowitz and Stegun*, 1972, p. 260].

The first two distributions are utilized extensively in practical applications. A 'hard' cutoff for the maximum moment (magnitude) is used in these expressions: in case (a) for the cumulative distribution function (CDF), and in case (b) for the PDF (probability density function). The two latter distributions apply a 'soft' exponential taper to the distribution tail: in case (c) to the CDF, and in case (d) to the PDF.

3.2. Empirical evidence: Moment-frequency relation

Pacheco et al. [1992], *Okal and Romanowicz* [1994], *Triep and Sykes* [1997] and others (see more references in the works by *Main* [2000] and *Leonard et al.* [2001]) argue that the β-value (3) increases from 2/3 to 1.0 over the moment range $M = 10^{17.25} - 10^{21}$ Nm ($m = 5.5 - 7.5$). They believe the finite thickness of a seismogenic crust explains this change.

To demonstrate the lack of scale breaking in the moment-frequency distribution, we show in Figs. 2 several curves for earthquakes in subduction zones with various focal mechanisms [*Bird*, 2003; *Bird and Kagan*, 2004] listed in the Harvard catalog. Since tectonic and other conditions on both sides of the boundary differ significantly, one expects the earthquake size distribution to differ also. We classify earthquakes by their focal mechanisms: thrust events have a T-axis which is more vertical than B or P. Similarly, normal earthquakes have a P-axis and strike-slip earthquakes have a B-axis more vertical than other axes, respectively. In addition, we subdivide the earthquake distribution into two groups: one on the ocean and one on the continental side of the subduction boundary. The β-values for all the samples are statistically indistinguishable and correspond to the universal value for the exponent [*Kagan* 2002a;b and *Bird and Kagan*, 2004].

The strike-slip earthquake distribution (Figs. 2A) is of special interest; according to the standard interpretation, their rupture width should approximately equal the thickness of the seismogenic upper crust. Thus, we expect the distribution to exhibit a break at about $10^{18} - 10^{19}$ Nm ($m = 6.0 - 6.7$). *Pacheco et al.* [1992] suggest that the b-value should change from 1.0 to 1.5 (corresponding limits are 2/3 to 1.0 for the β-value) at this magnitude range. No break of such amplitude is observed in the plots, at least by inspection. *Sornette et al.* [1996] discuss more rigorous testing techniques for the break in the magnitude-frequency relation. Closely inspecting the spatial distribution of the strike-slip earthquakes indicates that they are not concentrated in any of the subduction zones. Hence the absent break is not due to the seismicity alone in one or two subduction zones.

The tectonic structure in subduction zones may be very complex (i.e. the seismogenic crustal thickness highly variable) so that any systematic variation of rupture width may not be discernable. However, only subduction zones yield a sufficient number of earthquakes for statistical comparison. The absence of a break in scaling relation for strike-slip earthquakes can also be demonstrated by *Kagan* [2002c] results on the relation between the aftershock zone length and the mainshock magnitude. Strike-slip events exhibit no change in correlation behaviour up to magnitude $m \approx 8$ mainshocks (see more in Subsection 4.2).

Thrust earthquakes (Figs. 2B) demonstrate a similar pattern: there is no observable statistical difference in these diagrams. The upper observational curve decay (Fig. 2B) for the largest earthquakes ($M > 10^{20}$ Nm, $m > 7.7$) is caused by the upper bound for moment distribution (the maximum or corner magnitude. This decay is not seen in the lower curve (Fig. 2B), perhaps because its number of earthquakes is small. *Bird and Kagan* [2004] discuss the corner magnitude distribution for global earthquakes in various tectonic zones.

4. Earthquake scaling

To relate the moment-frequency law to observed geometrical properties of earthquake rupture and its statistics, we should know the relationship between these variables. This relation depends on earthquake scaling: the connection between the moment and rupture length, width, and slip. If we know or assume the scaling relation, we can then calculate the distribution of earthquake geometrical parameters by extending the moment-frequency relation.

4.1. Theoretical principles

Earthquake rupture is characterized by three geometric quantities: length of the rupture, L, width W, and average slip, u. The seismic moment is expressed through these quantities as [*Scholz*, 2002]

$$M = \mu u W L, \tag{8}$$

where μ is an elastic shear modulus. The empirical connection between the length and the moment M is expressed as

$$M \propto L^d, \tag{9}$$

i.e., M is proportional to L^d. From the scaling arguments and the observational evidence, it is generally agreed that $d = 3$ for small and moderate earthquakes whose size does not exceed the thickness of seismogenic layer [*Scholz*, 1997; 1998; *Romanowicz*, 1994; *Abercrombie*, 1995; Romanowicz and Ruff]. Since the stress or strain drop is generally assumed to be independent of M and the rupture unbounded, these variables should depend on the moment only

$$L,\ W,\ u \propto M^{1/3}. \tag{10}$$

Let us consider the slip distribution at a particular single site on the Earth's surface along the San Andreas fault. Since total slip can be partitioned between the major fault (the San Andreas in our case) and subsidiary faults, slip distribution is for a thin slice orthogonal to the San Andreas fault. Most of the total moment is released by the largest earthquakes, $M > 10^{19.5}$ Nm ($m > 7.0$) [*Brune*, 1968; *Kagan*, 2002a]; for these large earthquakes the rupture is usually considered confined to the upper crust layer of thickness W [*Scholz*, 1997; 1998; *Romanowicz*, 1994; *Wells and Coppersmith*, 1994; *Bodin and Brune*, 1996; *Stock and Smith*, 2000]. Thus, if

$$W = W_0 = \text{const}, \tag{11}$$

the rupture can be characterized by two geometric quantities: length L, and average slip, u.

Main [2000] and *Leonard et al.* [2001] discuss various methods of investigating geometrical scaling of the earthquake rupture. They propose evidence for a break in the scaling corresponding to the brittle-plastic transition at the base of the crust. Below we briefly review both of these relations: geometrical features of earthquakes and a supposed break in the magnitude(moment)-frequency relation.

The expressions above (8-11) implicitly assume that the hypocenter or centroid depth distribution is uniform over the thickness of the seismogenic layer – otherwise the width W is not properly defined. In reality, earthquake depth distribution is highly non-uniform. In Fig. 3 we show the depth histogram for one of the southern California catalogs [*Shearer et al.*, 2003], arguably the catalog with the most accurate earthquake locations. Most of its earthquakes are concentrated within the upper 2-12 km zone. However, slip inversions for several large earthquakes in California and elsewhere [*Mai and Beroza*, 2002] show that their slip distributions extend to greater depth. We know that slip inversions are not well constrained, especially for the lower part of the rupture width. Thus, the exact slip distribution over depth still needs to be established.

Several studies (see, for example, *Mori and Abercrombie* [1997]; *Gerstenberger et al.* [2001]; *Wyss et al.* [2004]) suggest that the magnitude-frequency relation varies with depth. In assuming the simple G-R law (2) these authors

show that the b-value significantly decreases with depth. However, *Kagan* [2002a, p. 539] argues that this decrease may be caused by an inappropriate use of relation (2) for approximating earthquake size distribution. If the maximum earthquake size is taken into consideration (Equations 4–7), a more reasonable explanation for the apparent b-value change would be an increase in the maximum size with depth [*Kagan*, 2002a, p. 538]. Centroid depth for a large earthquake on a vertical fault cannot be smaller than a half of the rupture width; inspecting seismic maps [like Fig. 2 in *Wyss et al.*, 2004] suggests that hypocenters of larger events are on average deeper than those for small earthquakes.

4.2. Empirical evidence: Length scaling

Although other parameters of rupture have been correlated with the seismic moment, rupture length is determined with better accuracy. This accuracy is reflected, for example, in a higher correlation coefficient of M versus L, as compared to the correlation of the moment with W, or u [*Wells and Coppersmith*, 1994]: $\rho = 0.95$ for the first case, and $\rho = 0.84$ and $\rho = 0.75$ for the second and third case, respectively. Thus, here we use only the M versus L correlation.

Two models are usually proposed for length scaling of large earthquakes. The W-model [*Romanowicz*, 1994, and references therein] assumes that slip is proportional to the rupture width W and thus is constant as long as the Equation (11) holds. The second or L-model [*Scholz*, 1997; 1998, and references therein] assumes that $u \propto L$. According to the W-model $d = 1$, whereas the L-model requires $d = 2$ (see Equation 8).

Kagan [2002c] investigated the distribution of aftershock zones for large earthquakes in global catalogs (scalar seismic moment $M \geq 10^{19.5}$ Nm, moment magnitude, $m \geq 7$). How the aftershock zone length, l, depends on earthquake size was studied for three representative focal mechanisms: thrust, normal, and strike-slip. It was found that all earthquakes show the same scaling ($M \propto l^3$). No observable scaling break or saturation occurs for the largest earthquakes ($M \geq 10^{21}$ Nm, $m \geq 8$). *Henry and Das* [2001] obtained an analogous scaling result. It is natural to assume that the aftershock zone length l is equal or proportional to the rupture length L. It seems that earthquake geometrical focal zone parameters are self-similar.

Preliminary data on the recent (2004/12/26) Sumatra great earthquake as well as addition of 2001-2004 earthquake catalogs allow us to extend *Kagan* [2002c] results. New regression curves (see http://scec.ess.ucla.edu/~ykagan/scal_update_index.html) show that $M \propto l^3$ dependence continues up to $m = 9$ earthquakes. Although the Sumatra earthquake is of thrust type, a few large $m \approx 8$ strike-slip events occurred in the 2001-2004 period. Estimated regression parameters for strike-slip and normal earthquakes are similar to those of thrust events, supporting the conjecture that the scaling relation is identical for earthquakes of various focal mechanisms.

4.3. Earthquake scaling relations

As the discussion above shows, geometrical scaling relations still challenge our understanding. The major difficulty in studying L, W, and u is that these quantities are often not subject to direct measurement, especially for earthquakes occurring under the ocean. Seismic moment is the best statistically studied variable among the earthquake scaling parameters. Therefore, we may try to infer statistical properties of other geometrical quantities by using their relations to the moment. If the assumed functional dependence between the moment and a variable x has a form

$$x = f(M), \tag{12}$$

then the PDF for x can be expressed as

$$\varphi_x(x) \;=\; \varphi_M\left[f^{-1}(x)\right] \left|\frac{\partial\left[f^{-1}(x)\right]}{\partial x}\right|, \tag{13}$$

where φ_M is the PDF of the seismic moment and $f^{-1}(x)$ is the inverse function of (12).

If x itself has a power-law dependence on the moment, say

$$x \;\propto\; M^{1/\nu} \quad \text{or} \quad M \;\propto\; x^{\nu}, \tag{14}$$

then for the scale-invariant part of the moment PDF (Equations 4, 5, 6, 7) we obtain the following relations for variable x

$$\varphi(x) \;\propto\; \left(x^{\nu}\right)^{-1-\beta}\, x^{\nu-1} \;=\; x^{-1-\nu\beta}, \tag{15}$$

i.e., the x-variable is power-law distributed with the exponent value $\nu\beta$. Using (9) for the rupture length, we obtain

$$\varphi(L) \;\propto\; \left(L^d\right)^{-1-\beta}\, L^{d-1} \;=\; L^{-1-\beta d}. \tag{16}$$

Hence, for earthquakes smaller than the maximum or corner moment M_x, the length L is distributed according to a power-law (see Table 1 for exponent values). Similarly, the PDF for the other variables, like width W and average slip u can be calculated as long as they follow the same proportionality relations as the moment (see Equation 10).

If we assume that (11) is true,

$$L = L_0\left(\frac{M}{M_0}\right)^{1/d}, \tag{17}$$

and,

$$u = u_0\left(\frac{M}{M_0}\right)^{(d-1)/d}, \tag{18}$$

where M_0, L_0, and u_0 are the seismic moment, length, and average slip for a reference earthquake, taken here for illustration to be $M_0 = 10^{19.5}$ Nm ($m = 7$), i.e., the smallest earthquake for which its rupture width reaches the maximum value W_0. For an $m7$ earthquake, assuming the width W_0 of 15 km and elastic modulus μ equal to 30 GPa [*Scholz*, 2002, p. 207], we take $u_0 = 1.87$ m and $L_0 = 37.5$ km. We use these reference earthquake parameters in discussion below as an illustration. The derivations can be easily repeated using other values.

The ratio $\theta = u/L$ is an important parameter which determines the stress drop $\Delta\sigma$

$$\Delta\sigma \;=\; C\mu\theta, \tag{19}$$

where C is a coefficient of the order of unity [*Scholz*, 2002, Eq. 4.29].

Using (17) and (18) we obtain the following expression for θ

$$\theta \;=\; \frac{u_0}{L_0}\left(\frac{M}{M_0}\right)^{(d-2)/d}. \tag{20}$$

From this equation, the stress drop depends on the moment of an earthquake with the exponent equal to $-1/3$, 0, and $1/3$ for $d = 1.5$, 2.0, and 3.0, respectively. The independence of the stress drop from earthquake size seems well established [*Scholz*, 2002; *Abercrombie*, 1995]. Therefore,

assumption (11) leads us to accept the L-model of scaling ($d = 2$).

However, assumption (11) may not be true, as suggested by the evidence discussed above, then using (10) we obtain for $d = 3$

$$\theta \;=\; \frac{u_0}{L_0}\,, \tag{21}$$

i.e., the stress drop is again constant.

From (18) similar to (13) and (16), we obtain the scale-invariant part of the PDF for the slip

$$\varphi(u) \;\propto\; \left[u^{d/(d-1)}\right]^{-1-\beta}\, u^{1/(d-1)} \;=\; u^{-1-\beta d/(d-1)}\,. \tag{22}$$

Hence for earthquakes smaller than the maximum or corner moment M_x, slip u is distributed according to a power-law (see Table 1).

Table 1 shows the exponent values for three choices of the moment-frequency exponent. Value $\beta = 2/3$, corresponding to the G-R $b = 1$, is the most often quoted quantity. *Kagan*'s [2002a;b] results and those by *Bird and Kagan* [2004] suggest that a slightly lower β-value of 0.63 characterizes shallow earthquake seismicity. The index value $\beta = 0.6$ may be appropriate for shallow earthquake sequences or deep earthquakes [*Kagan*, 1999]. Finally, $\beta = 1/2$ is the theoretically derived value [*Vere-Jones*, 1976].

5. Earthquakes at a specific site

Most known statistical distributions for earthquake size (magnitudes or seismic moment) are constructed for areas or regions. However, earthquake rupture extends over the length of a fault. Thus, if we are interested in earthquake phenomena observed at a particular point on a fault, we need to 'translate' these distributions into a site-specific form. Large earthquakes have a higher probability of intersecting the site than smaller ones, and this probability should be accounted for. Below we calculate site distributions for seismic moment and earthquake slip.

5.1. Earthquake moment distribution at a specific site

To calculate the distribution of the seismic moment at a single site $v(M)$, we consider two cases: a potential width of the rupture W is greater than W_0 – the width of the seismogenic zone – and $W \le W_0$. In the first case we multiply the distribution density function of the seismic moment $\phi(M)$ by the length of the rupture $L(M)$ as described by Equation (8). The probability of an earthquake rupture transecting the fault system at a certain site is proportional to the length

$$v(M_s) \;\propto\; L(M)\phi(M) \;=\; M^{1/d}\phi(M). \tag{23}$$

Using the scale-invariant part of the $\phi(M)$ expression in (23), we obtain

$$v(M_s) \propto M^{-1-\beta+1/d}. \tag{24}$$

Although the PDF of the moment distribution has a power-law form similar to those considered in Section 3.1, the power exponent is smaller. Actually for $d = 1.5$, the logarithmic density is uniform over the scale-invariant segment (see Table 1 for exponent values).

For $d = 2$ the value of the exponent (1/6) is derived by *Anderson and Luco* [1983]: since they use the magnitude rather than the moment, the exponent in (24) needs to be multiplied by 1.5, resulting in 1/4. For $d = 3$ the exponent value is only two times smaller than the value of the moment-frequency or magnitude-frequency relations (1/3 and 1/2, respectively).

Anderson and Luco [1983] also argue that since the value of the exponent for the site-specific distributions is significantly smaller than that for the area-specific relations, this difference may also explain differences in the paleoseismic distributions (site-specific) and distributions of instrumental earthquake catalog data (usually area-specific). Moreover, as we suggest in Section 4.1, because of a lack of earthquakes near the Earth's surface and the possible relative reduction of large earthquakes near it, it seems likely that only large earthquakes rupture the surface. For example, if we assume that no earthquakes occur in the crust's upper 1.5 km layer, then the smallest earthquake that could rupture the surface would be about $m5$. Since the total displacement of seismogenic crust at any depth interval over long time should be uniform, this would mean that the slip of large earthquakes should "catch up" on the slip deficit at the Earth's surface left by smaller events, i.e., large earthquake slip at the surface should be on average greater than the slip in the crust middle layers. If this conjecture is true, then the slip and, by inference moment distributions in paleoseismic studies would significantly differ from the power-law (like Equation 3), which explains instrumental seismological data. This deviation may provide a misleading evidence in support of claims in the characteristic earthquake model.

In general, the value of the exponent equal to 1.0 means that in the logarithmic scale the total sum for a variable is uniformly distributed. For example, the total length (L_s) for $d = 3$ and $\beta = 2/3$ is equal for all magnitudes. The value of the exponent equal to 0.0 means that the same condition is satisfied for a linear scale.

In the second case ($W < W_0$), several earthquakes are needed to fill out the vertical zone of length $W(M)$. Thus, in addition to (24) we multiply the density by a term $W(M) \propto M^{1/d}$

$$v(M) \;\propto\; L(M)\,W(M)\phi(M) \;=\; M^{2/3}\phi(M), \tag{25}$$

where we use $d = 3$ as in Equation (10), appropriate for this case. We assume that small earthquakes are distributed uniformly in width W_0.

The latter expression may be considered as a PDF of a fault surface covered by earthquake ruptures

$$v(S(M)) \;\propto\; M^{-1-\beta+2/3}, \tag{26}$$

i.e., for $\beta = 2/3$, earthquakes of any magnitude or log moment range cover the same total surface [*Rundle*, 1989].

In Appendix A we derive several formulas of the complementary moment functions for cases (a) and (b). The expressions for cases (c) and (d) can be obtained by the same method, not shown because of their length. In Fig. 4 we show several examples of these functions. The functions are not normalized in this case. It is to be expected that for a smaller value of the d-exponent the rupture length of large earthquakes will increase. Thus, more ruptures will intersect the site.

In the diagram we adjust the maximum moment M_x or the corner moment M_c of the distribution according to Eq. 7 by *Kagan* [2002b], so that the total moment rate $\dot{M}$ is identical for all four distributions: $M_x = 10^{21}$, 3.38×10^{21} and $M_c = 1.40 \times 10^{21}$, and 4.74×10^{21} Nm, for models (a)-(d), respectively. These moment values correspond approximately to magnitude values $m_x = 8.0$, 8.35, 8.10, and 8.45, appropriate, for instance, to southern California (*Jackson et al.* [1995]; *Field et al.* [1999]). *Kagan* [2002b, his Fig. 2 and Eq. 21] estimates that for such conditions, $m < 7$ earthquakes contribute about 21% of the total seismic moment. *Bird and Kagan* [2004] also obtained the corner magnitude

(case (c) – see Equation 6) values of $m_{cm} = 8.04^{+0.47}_{-0.21}$ for analogous tectonic regions (continental transform boundaries) in global earthquake distribution.

Comparing the moment-frequency log-log plots (for example, see Fig. 1 in *Kagan* [2002a]) with Fig. 4, we see another significant difference between the moment distributions for an area and a site-specific distribution: even for the characteristic model, the cumulative curve is no longer linear in a log-log plot. The reason is that site-specific distributions are defined for earthquakes close to the upper limit of the distribution. But the right-hand tail of the cumulative distributions is not linear for area-specific curves. For the characteristic law we adjusted the number of characteristic events in such a way as to produce a linear area-specific curve. This adjustment is no longer valid for a site-specific distribution.

For illustration we calculate the number of earthquakes at a site for conditions similar to southern California, setting in Equation (A4) $M = M_0 = 1$. We take $\alpha_0 = 0.04$ (rate of $M \geq 10^{19.5}$ Nm, $m \geq 7$ earthquakes, see Fig. 1), the total length of the fault system $L = 700$ km, and $\beta = 2/3$ [*Kagan*, 1996]. To illustrate, for the truncated Pareto distribution

$$n \;=\; \alpha_0 L_0 \frac{\beta d}{L\,(\beta d - 1)} \times \frac{M_{xp}^{\beta}}{M_{xp}^{\beta} - 1}\,\left[1 - M_{xp}^{-\xi}\right], \quad (27)$$

$M_{xp} = 106.7$, if we normalize $M_0 = 1$. Then for $d = 3$ we obtain 3.61, 3.54, 3.52, and 3.5 (cases a-d, respectively) events that rupture an arbitrary site per millenium. The difference between various distributions is insignificant. For $d = 2$ the numbers are approximately 4.9, and for $d = 1.5$ the numbers are around 7.0. The obtained numbers of earthquake ruptures are comparable with the number of $m \geq 7$ earthquakes found during paleoseismic explorations of the San Andreas fault (e.g., *Sieh et al.* [1989]; *Weldon et al.* [2002]; see also Fig. 9).

5.2. Earthquake slip distribution at a specific site

Again, assuming $W = W_0$, as in (16) using (24) as the PDF for distribution (φ_M), we obtain the following site-specific relations for the rupture length (L_s)

$$\varphi(L_s) \;\propto\; \left(L_s^d\right)^{-1-\beta+1/d} L_s^{d-1} \;=\; L_s^{-\beta d} \;=\; L_s^{-1-\kappa}\,. (28)$$

The length L_s is distributed according to a power-law (see Table 1).

The site-specific relations in the case of $W = W_0$, for the rupture slip (u_s)

$$\begin{aligned}\varphi(u_s) \;&\propto\; \left[u_s^{d/(d-1)}\right]^{-1-\beta+1/d} u_s^{1/(d-1)} \\ &=\; u_s^{-1-(\beta d-1)/(d-1)} \;=\; u^{-1-\zeta}\,, \end{aligned} \quad (29)$$

the slip u_s is also distributed according to a power-law (see Table 1). In Fig. 5, we display complementary functions for $d = 2.0$ (see Appendix B for appropriate formulas). We use the same maximum magnitude quantities as in Fig. 4. The distributions are similar over much of the slip range. According to the gamma law, in some rare cases the slip magnitude can reach almost 30 m.

In the second case ($W < W_0$), several earthquakes $n \propto M^{1/3}$ are needed to fill out the rupture width. We assume that their slip distribution is the same as that for larger ($m \geq 7$) events. Each of these smaller events on average contributes u/n slip to total displacement of the surface.

In Figs. 6A and 6B we display the distributions of the total slip (see Appendix C for the expressions). In the first plot (Fig. 6A) it is assumed that all surface slip is due to large ($m \geq 7$) earthquakes; in the latter picture we estimate the contribution of smaller events. For the reasons explained above (Section 4.1), the slip accumulated due to small and moderate ($m < 7$) earthquakes close to the Earth's surface is probably released during the rupture of large events.

In both figures, the distribution of the total slip for $d = 1.5$ is linear, demonstrating that in each linear interval earthquakes contribute an equal amount to the total slip budget. But the length of the rupture for $d = 1.5$ is too large for an $m = 8.35$ earthquake, whose $L = 840$ km. For the greater d-values the larger part of the slip total is released by more extensive slip events. For example, for $d = 3$ about 50% of the total slip is caused by slips in individual earthquakes exceeding 15 m. The largest slip in the $d = 3$ case exceeds 50 m for the largest earthquakes: a value that seems unrealistic, especially for the gamma distribution.

However, if we assume that $d = 3$ and allow for an unlimited width W, the total slip for $m = 8.35$ earthquake is only 8.87 m, although its width should reach 71.1 km, and the length $L = 177.9$ km. These parameter values may be appropriate for subduction zones. For such $m > 8$ earthquakes the scaling is most likely a mixture of condition (11) and unlimited W.

6. Seismic moment and slip release in time

The seismic moment and slip distributions obtained in previous sections cannot be used for theoretical modeling and practical purposes of seismic hazard evaluation without a proper understanding of earthquakes occurrence in time. Unfortunately, there is no present consensus on even basic facts about the temporal distribution of the large earthquakes or principles for their mathematical representation. Below we briefly discuss available data and their interpretation and show one example of applying results of this work.

6.1. Temporal evolution of seismic moment release

There are several models for stress accumulation and release by earthquakes. Most of these models assume that stress is scalar, i.e., the tensor properties of stress are disregarded. These models are descendants of *Reid's* [1910] "Elastic rebound theory." Two recent modifications of this model are presented by *Shimazaki and Nakata* [1980]: the "time-predictable" and "slip-predictable" earthquake occurrence hypotheses. In the former, stress accumulates until it reaches an upper critical value and is then released by earthquakes of various magnitudes. In the latter model, the release of stress during an earthquake is limited by a lower critical quantity; following stress release, it accumulates until a new earthquake is triggered. In both models the total variation of stress cannot exceed the moment released by the largest earthquakes. It is also assumed that after such an earthquake, the tectonic stress level is close to zero [*Jaumé and Sykes*, 1996, their Fig. 4].

The often preferred time-predictable model implies that the probability of a new earthquake is lower, especially after a large event, since the stress field is significantly depleted: a stress shadow is created. This conclusion contradicts the universally observed clustering of shallow earthquakes. The most obvious manifestation of such clustering is aftershock sequences subsequent to strong events [*Kagan and Jackson*, 1999; *Rong et al.*, 2003].

A commonly used explanation of the contradiction is that the shadow effects start following an aftershock sequence and outside the aftershock zone. However, it is difficult to draw temporal and spatial boundaries for aftershock sequences. Some of these sequences (such as the ones following the 1952 Kern County earthquake, or the Nobi earthquake of 1891, see *Utsu et al.* [1995]) are still active after several

decades. There are many indications that intraplate earthquakes, where the tectonic deformation rate is low, have aftershock sequences decades and centuries long [*Ebel et al.*, 2000]. There are also distant aftershocks, which further complicate determination of the aftershock zone.

Another attempt at explaining the above contradiction is that clustering is a property of small earthquakes only; large events rupturing the whole crust follow a time- or slip-predictable model. Yet *Kagan and Jackson* [1999] show that even $M \geq 10^{20.25}$ Nm ($m \geq 7.5$) earthquakes continue to exhibit time-distance clustering. The time interval between closely spaced pairs of earthquakes is significantly less than the time span needed for the plate motion to accumulate the strain released by the first event. Some $M \geq 10^{20.25}$ Nm ($m \geq 7.5$) earthquake pairs listed by *Kagan and Jackson* [1999] clearly qualify as members of a foreshock-mainshock-aftershock sequence, which suggests that strong earthquakes can recur at a small time interval in essentially the same area. *Pérez and Scholz* [1997] demonstrate that very large earthquakes $M \geq 10^{21.75}$ Nm ($m \geq 8.5$) are still accompanied by foreshock/aftershock sequences that include large earthquakes. Hence these earthquakes do not fully release accumulated deformation. It is still possible that earthquakes can become large enough to deter others at some greater threshold. However, if an earthquake releases only a small part of tectonic stress, then many assumptions of earthquake temporal behavior need revision.

To illustrate possible stochastic variations in the seismic moment release, we display in Fig. 7 four simulations of the process. Their earthquake size distribution is assumed to follow the truncated density G-R law (5), with the maximum moment equal to 10^{21} Nm ($m = 8$) and the minimum size earthquake equal to 10^{18} Nm ($m = 6$). The earthquake temporal distribution is assumed to be governed by the Poisson law with the rate of occurrence of one event per unit of time. We use the technique described by *Kagan* [2002a, his Eq. 40] to simulate truncated Pareto distribution for moment, and the standard methods to obtain the Poisson variable.

The curves' behaviors significantly differ from the idealized pictures of stress-time history in the time- or slip-predictable models [*Jaumé and Sykes*, 1996, their Fig. 4]. However, some of the trajectories (like the solid curve in Fig. 7) can be interpreted using these hypotheses. Three of the four series in Fig. 7 imply stress buildups that look implausible.

The possible reason for such moment behavior is use of the Poisson process to model earthquake occurrence. The problem with the Poisson distribution utilized in Fig. 7 is that regional stress accumulation would change drastically, since the Poisson process allows a potentially infinite accumulation of strain in a region. Clearly, some modification of Poisson model strain accumulation is necessary. *Zheng and Vere-Jones* [1994] propose a stochastic version of the elastic rebound model for describing large earthquake occurrence within a seismic region. This model replaces a deterministic 'hard' threshold with a soft statistical critical cut-off to allow within certain stochastic limits clustering of large earthquakes. Further development of this model and review of results is presented by *Bebbington and Harte* [2003]. However, the results of this hypothetical application are still ambiguous, perhaps because the model does not fully incorporate earthquake spatial parameters. Thus, the problem persists. Are the largest earthquakes quasi-periodic or clustered? Is one pattern changed by another for large enough time intervals?

6.2. Slip accumulation in time

Difficulties in describing earthquake temporal distribution remain for slip accumulation as well. *Chery et al.* [2001] discuss many qualitative examples of long-term clustering for large earthquakes. *Rockwell et al.* [2000] and *Dawson et al.* [2003] discover a similar temporal earthquake clustering in eastern California. These researchers define clustering as a deviation of earthquake occurrence from a periodic or quasi-periodic pattern. In statistics, temporal clustering is normally assumed if a point process has a larger coefficient of variation than the Poisson process [*Kagan and Jackson*, 1991, their Fig. 1]. For example, *Sieh et al.*'s [1989] results are usually interpreted as evidence for earthquake clustering, although they find that the Poisson hypothesis cannot be rejected as a model for the temporal event series they describe. Generally, paleoseismic investigations cannot distinguish earthquakes occurring closely in time. Hence, their coefficient of variation estimates should be biased towards smaller quantities: a more periodic pattern.

Quantitative studies of earthquake temporal occurrence [*Kagan and Jackson*, 1991; 1999] suggest that strong earthquakes are more clustered than a Poisson process. Such clustering can presently be established for instrumental catalogs: for time intervals of a few decades at maximum. Paleoseismic investigations [*Rockwell et al.*, 2000; *Dawson et al.*, 2003] also suggest that earthquakes follow a long-term clustering pattern at least in regions of slow tectonic deformation. Average slip rates are known to be stable for most significant faults over 10,000 to 10^6 years. But earthquake long-term clustering implies that the rates should fluctuate at least on the order of hundreds or thousands of years.

Recent paleoseismic investigations of slip distribution on California faults [*Weldon et al.*, 2002; *Scharer et al.*, 2003] cast doubt on the quasi-periodic model of slip accumulation. Although the Poisson distribution for slip events on earthquake faults may be incorrect over long time intervals, this distribution approximates the observed temporal sequences. Thus, as a provisional model of seismic temporal behavior, we suggest that at relatively short time intervals (less than a millenium) strong earthquakes are clustered. For longer time intervals (several thousand years) their pattern can be approximated by the Poisson process, and, finally, for even longer times 2-D continuum variants of the stochastic stress release model *Zheng and Vere-Jones* [1994] may fit better.

In Fig. 8, we show four examples of synthetic slip history obtained by Monte-Carlo simulations. These realizations demonstrate a significant random variability of slip release when one assumes that their time distribution is Poisson and the slip distribution is a power-law. Simulation methods are analogous to that used in Fig. 7. We also show the Gaussian approximations of random uncertainties [*Kagan*, 2002a, his Eq. 10; *Zaliapin et al.*, 2005, their Eqs. 60 and 61]

$$\mu_y = \begin{cases} \frac{\zeta}{1-\zeta}\left(y^{1-\zeta}-1\right)/\left(1-y^{-\zeta}\right), & \zeta \neq 1, \\ \log(y)/(1-y^{-1}), & \zeta = 1, \end{cases} \tag{30}$$

$$\sigma_y^2 = \begin{cases} \frac{\zeta}{2-\zeta}\left(y^{2-\zeta}-1\right)/\left(1-y^{-\zeta}\right) - \mu_y^2, & \zeta \neq 2, \\ 2\log(y)/\left(1-y^{-2}\right) - \mu_y^2, & \zeta = 2 \end{cases} \tag{31}$$

where μ_y and σ_y^2 are the conditional mean and variance of each normalized summand, given the restriction on the maximum slip y. These Gaussian estimates reasonably approximate the accumulated variable; see more in [*Zaliapin et al.*, 2005].

6.3. Example: Slip statistical distribution, San Andreas fault at Wrightwood, CA

Weldon et al. [2002] (see also *Scharer et al.* [2003]) present a detailed analysis of earthquake slip history on the San Andreas fault at Wrightwood, CA. In Fig. 9, we show the statistical distribution of slip events approximated by a power-law (Pareto distribution). Since small slips may not be represented fully in the soil record, we employ a threshold slip

1.5 m, similar to an approximation of the earthquake seismic moment. Unfortunately, it is difficult to reliably estimate the slip threshold as can be done for the magnitudes. As Section 4.1 explained, it seems likely that rupture at the Earth's surface is caused mostly by large earthquakes. Therefore, a deficit of small slips or an almost complete absence is to be expected. *Liu et al.* [2004] also find that the smallest offset at the Carrizo Plain (San Andreas fault) is 1.4 m. Hence, we assume that the slip record is complete only for slip events larger than 1.5 m.

The approximation of the slip distribution by the Pareto law yields $\zeta = 1.52 \pm 0.51$. When comparing these ζ-values to the theoretical estimates in Table 1, a few assumptions should be made. In Fig. 9, the fault slip is measured at a point on the San Andreas fault. The distribution may differ from that of average slip u calculated in Table 1. *Rockwell et al.* [2002] indicate that surface slip may drastically change over relatively small distance over fault. *Ward* [2004] proposes approximating slip distribution along a fault by the Brownian bridge; applicability of this model needs to be explored. Moreover, as mentioned above, small slips have a larger chance of being overlooked, thus biasing the input data. Nevertheless, the obtained ζ-value is compatible with $\zeta = 1$ for the site-specific value shown for $M^{1/3}$ dependence (Table 1).

Fig. 10 shows the slip history at Wrightwood with several uncertainties estimates. For the truncated distribution we assume that the maximum slip is 15 m. *Bird and Kagan* [2004] find that for continental transform faults the corner magnitude estimate is $8.04^{+0.47}_{-0.21}$ (more in Section 5.1). An average slip of 15 m is consistent with this moment magnitude value. We also estimate the uncertainties of slip accumulation by a simulation performed similarly to that of Fig. 8. However, to estimate upper and lower bounds, we used 10,000 instead of 4 realizations as in Fig. 8. For this choice of parameters, the Gaussian estimates (30, 31) reasonably approximate those obtained through simulation.

7. Discussion

Three problems must be solved to explain earthquake recurrence: (a) the degree of allowed stress accumulation in seismic zones; (b) the distribution of strain release by earthquakes of various sizes; and (c) the distribution of stress release along the fault during a large earthquake. The continuum/block character of Earth deformation (Section 2) requires that all these problems be resolved within a framework of the 2-D or 3-D stochastic field process. As explained in the Introduction, both observational data and a theoretical foundation are not yet sufficient for solving the problems.

We tried to solve a simpler problem: distribution of earthquake slip at tectonic fault sites where the slip is sufficiently concentrated to be measured by paleoseismic methods. Even this simpler task cannot be fully accomplished because several components of the earthquake process are not adequately known. Among these unknown or contested features are:

1. Temporal distribution for large and great earthquakes for time periods of decades, centuries, and millenia.
2. Earthquake scaling for events with $m \geq 8$.
3. Dependence of earthquake surface slip on both the nonuniformity of earthquake depth distribution and a possible change of magnitude-frequency relation with depth.
4. Statistics of the slip distribution along fault rupture [cf. *Mai and Beroza*, 2002; *Ward*, 2004].

The scheme of the stress evolution discussed above raises two related questions. What is the maximum moment of earthquakes? What are the relations between the stress levels and earthquakes? Apparently these problems cannot be solved with available data, but accumulating paleoseismic results and space-geodetic measurements may provide the necessary input.

Although solving the earthquake slip distribution problem in this paper cannot be considered complete and fully self-consistent, our theoretical results may be used to interpret various observational data. Even if consensus on earthquake size distribution, scaling of earthquake geometric parameters and earthquake temporal behavior is not yet there, the derived formulas can be applied to different sets of assumed distributions.

Finally, we briefly comment on issues needing resolution before we can create a viable model of the Earth's surface deformation to compare with new and future GPS and InSAR measurements:

(a) The fractal nature of fault systems should be explicitly used in constructing the model.

(b) Earthquake focal mechanisms should be included as an intrinsic part of the model (see Section 2). This would greatly increase the model's complexity, since we would have to deal with tensor-valued stochastic processes.

(c) The power-law distributions that control earthquakes need to be integrated with the model; that improvement will necessitate using stable statistical distributions: a rapidly developing discipline in mathematical statistics [*Zaliapin et al.*, 2005].

8. Conclusions

We have analyzed the distribution of earthquake size, geometrical scaling of earthquake rupture and temporal earthquake patterns to derive a possible distribution for average slip on extended faults. The results can be summarized as follows:

1. Earthquake slip is power-law distributed. The power-law exponents are derived as they depend on various assumptions.
2. Formulas are proposed to approximate slip at paleoseismic sites and evaluate uncertainties due to the statistical nature of slip accumulation and its size distribution.

Acknowledgments. I appreciate partial support from the National Science Foundation through grant EAR 00-01128, from CalTrans grant 59A0363, and from the Southern California Earthquake Center (SCEC). SCEC is funded by NSF Cooperative Agreement EAR-0106924 and USGS Cooperative Agreement 02HQAG0008. This work also is supported in part by the National Science Foundation under Grant No. DMS-0306526. The author thanks D. D. Jackson, F. Schoenberg and I. V. Zaliapin of UCLA and D. Vere-Jones of Wellington University for useful discussions. The comments by two reviewers as well as by the Associate Editor Joan Gomberg have significantly improved the presentation. I am also very grateful to Kathleen Jackson who edited the final manuscript version. Publication 821, SCEC.

APPENDICES:

Appendix A: Seismic moment distribution at a site

To calculate the distribution of the seismic moment at a site we assume that on a fault zone of total length L, the rate of earthquake with moment $M_0 = 10^{19.5}$ Nm ($m = 7$) or greater and rupture length $L_0 = 37.5$ km is equal to α_0 (see Section 4.3). The complementary moment function is then

$$\Upsilon(M) \;=\; \frac{\alpha_0 L_0}{L} \times C_1^{-1} \int_M^\infty x^{1/d} \phi(x) dx, \qquad \text{(A1)}$$

where $\phi(x)$ is defined by Equations (4), (5), (6), (7) and C_1^{-1} is a normalizing coefficient. Similar to the moment-frequency relation, the function $\Upsilon(M)$ shows the number of fractures caused by an earthquake with moment M at a fault site.

For the characteristic distribution

$$\begin{aligned} \Upsilon(M) \;&=\; \tfrac{\alpha_0 L_0}{L\,\xi d} \times [\beta d (M_0/M)^\xi - (M_0/M_{xc})^\xi] \\ &\qquad \text{for} \quad M_{xc} > M \geq M_0, \quad \text{and} \\ \Upsilon(M) \;&=\; 0 \quad \text{for} \quad M > M_{xc}\,, \end{aligned} \qquad \text{(A2)}$$

where $\xi = \frac{\beta d - 1}{d}$. Using Eq. 7 by *Kagan* [2002b] we can convert (A2)

$$\begin{aligned} \Upsilon(M) \;&=\; \tfrac{1-\beta}{\xi d} \times \dot{M}_0 M_0^{-\beta} M_{xc}^{\beta-1} \\ &\quad \times [\beta d (M_0/M)^\xi - (M_0/M_{xc})^\xi] \\ &\qquad \text{for} \quad M_{xc} > M \geq M_0\,, \end{aligned} \qquad \text{(A3)}$$

where $\dot{M}_0$ is the seismic moment rate on L_0.

For the truncated Pareto distribution,

$$\begin{aligned} \Upsilon(M) \;&=\; \tfrac{\alpha_0 L_0 \beta \eta_p}{L\,\xi} \times [(M_0/M)^\xi - (M_0/M_{xp})^\xi] \\ &\qquad \text{for} \quad M_{xp} > M \geq M_0, \quad \text{and} \\ \Upsilon(M) \;&=\; 0 \quad \text{for} \quad M \geq M_{xp}\,, \end{aligned} \qquad \text{(A4)}$$

where η_p is defined by

$$\eta_p = \frac{M_{xp}^\beta}{M_{xp}^\beta - M_0^\beta}\,, \qquad \text{(A5)}$$

Alternately,

$$\Upsilon(M) \;=\; \tfrac{1-\beta}{\xi d} \times \dot{M}_0 M_0^{-\beta} M_{xp}^{\beta-1} \times [(M_0/M)^\xi - (M_0/M_{xp})^\xi] \qquad \text{for} \quad M_{xp} > M \geq M_0\,. \qquad \text{(A6)}$$

If $\beta d = 1$, the above formulas need to be modified. For the characteristic distribution,

$$\begin{aligned} \Upsilon(M) \;&=\; \tfrac{\alpha_0 L_0}{L} \times [1 - \log(M_{xc}/M)] \\ &\qquad \text{for} \quad M_{xc} > M \geq M_0, \quad \text{and} \\ \Upsilon(M) \;&=\; 0 \quad \text{for} \quad M > M_{xc}\,, \end{aligned} \qquad \text{(A7)}$$

For the truncated Pareto distribution,

$$\begin{aligned} \Upsilon(M) \;&=\; \tfrac{\alpha_0 L_0 \beta \eta_p}{L} \times \log(M_{xp}/M) \\ &\qquad \text{for} \quad M_{xp} > M \geq M_0, \quad \text{and} \\ \Upsilon(M) \;&=\; 0 \quad \text{for} \quad M \geq M_{xp}\,, \end{aligned} \qquad \text{(A8)}$$

Appendix B: Slip distribution

The distribution density of the average slip is obtained from $v(M)$ (see Equations 18, 23), as

$$f(u) \;\propto\; v\left[u^{d/(d-1)}\right]\; u^{1/(d-1)}. \qquad \text{(B1)}$$

Inserting in (B1) appropriate expressions for seismic moment distribution, and integrating to obtain a cumulative function, we obtain the following formulas for the complementary function of displacement

$$\Psi(u) = C^{-1} \int_u^\infty f(x) dx. \qquad \text{(B2)}$$

To simplify the equations we normalize the displacement by dividing them by $u_0 = 1.87$ m; u_x is the slip corresponding to the maximum earthquake (normalized by dividing it by u_0).

For the characteristic distribution,

$$\begin{aligned} \Psi(u) \;&=\; \tfrac{\beta d\, u^{-\zeta} - u_{xc}^{-\zeta}}{\beta d\, u_0^{-\zeta} - u_{xc}^{-\zeta}}, \quad \text{for} \quad u_{xc} > u \geq u_0, \quad \text{and} \\ \Psi(u) \;&=\; 0 \quad \text{for} \quad u \geq u_{xc}\,, \end{aligned} \qquad \text{(B3)}$$

where

$$\zeta = \frac{\beta d - 1}{d - 1}\,, \qquad \text{(B4)}$$

hence $\zeta \geq 0$ for $d \geq 1/\beta$.

For the truncated Pareto distribution of the seismic moment,

$$\begin{aligned} \Psi(u) \;&=\; \tfrac{u^{-\zeta} - u_{xp}^{-\zeta}}{u_0^{-\zeta} - u_{xp}^{-\zeta}}, \quad \text{for} \quad u_{xp} > u \geq u_0, \quad \text{and} \\ \Psi(u) \;&=\; 0 \quad \text{for} \quad u \geq u_{xp}\,. \end{aligned} \qquad \text{(B5)}$$

For the gamma distribution of the seismic moment,

$$\begin{aligned} \Psi(u) \;&=\; \tfrac{C_1}{C_g} \left\{ \Gamma\left[1 - \tfrac{\beta d - 1}{d}, \left(\tfrac{u}{u_{xg}}\right)^{d/(d-1)}\right] \right. \\ &\quad \left. + \left(\tfrac{u}{u_{xg}}\right)^{(1-\beta d)/(d-1)} \exp\left[-\left(\tfrac{u}{u_{xg}}\right)^{d/(d-1)}\right] \right\}, \end{aligned} \qquad \text{(B6)}$$

where $\Gamma(a, x)$ is the incomplete gamma function (*Abramowitz and Stegun*, 1972, p. 260)

$$P(x, a) = \big(\Gamma(a)\big)^{-1} \int_0^x e^{-t} t^{a-1} dt, \quad \text{for} \quad a > 0\,, \qquad \text{(B7)}$$

where $\Gamma(a)$ is the gamma function (*Abramowitz and Stegun*, 1972, p. 260).

$$\begin{aligned} C_1 \;&=\; \beta \left(\tfrac{d}{1-\beta d}\right) \left(\tfrac{u_0}{u_{xg}}\right)^{(1-\beta d)/(d-1)} \\ &\quad \times \exp\left[\left(\tfrac{u_0}{u_{xg}}\right)^{d/(1-d)}\right], \end{aligned} \qquad \text{(B8)}$$

and

$$\begin{aligned} C_g \;&=\; C_1\, \Gamma\left[1 - \tfrac{\beta d - 1}{d}, \left(\tfrac{u_0}{u_{xg}}\right)^{d/(1-d)}\right] \\ &\quad + \tfrac{\beta d}{\beta d - 1}\,. \end{aligned} \qquad \text{(B9)}$$

If $\beta d = 1$, the above formulas need to be modified. For the characteristic distribution,

$$\Psi(u) = \frac{d-1+\log u_{xc} - \log u}{d-1+\log u_{xc} - \log u_0}, \quad \text{for} \quad u_{xc} > u \geq u_0, \quad \text{and}$$
$$\Psi(u) = 0 \quad \text{for} \quad u \geq u_{xc}. \qquad \text{(B10)}$$

For the truncated Pareto distribution,

$$\Psi(u) = \frac{\log u_{xp} - \log u}{\log u_{xp} - \log u_0}, \quad \text{for} \quad u_{xp} > u \geq u_0, \quad \text{and}$$
$$\Psi(u) = 0 \quad \text{for} \quad u \geq u_{xp}. \qquad \text{(B11)}$$

For the gamma distribution of the seismic moment,

$$\Psi(u) = E_1\left(\frac{u}{u_{xg}}\right) \Big/ E_1\left(\frac{u_0}{u_{xg}}\right) \quad \text{for} \quad u \geq u_0, \qquad \text{(B12)}$$

where $E_1(z)$ is an exponential integral (*Abramowitz and Stegun*, 1972, p. 228)

$$E_1(z) = \int_z^\infty t^{-1} e^{-t} dt. \qquad \text{(B13)}$$

We calculate this integral using the MATHEMATICA package (*Wolfram*, 1999).

Appendix C: Cumulative slip distribution at a site

The cumulative distribution of the total slip at a site can be expressed as follows: For the characteristic distribution of the seismic moment tensor,

$$\Phi(u) = C_2 \frac{u^{1-\zeta}-1}{u_{xc}^{1-\zeta}-1}, \quad \text{for} \quad u_{xc} > u \geq 1, \quad \text{and}$$
$$\Phi(u) = 1 \quad \text{for} \quad u \geq u_{xc}, \qquad \text{(C1)}$$

where

$$\zeta = \frac{\beta d - 1}{d-1}, \qquad \text{(C2)}$$

see (B4) and

$$C_2 = \beta \frac{1 - u_{xc}^{\zeta-1}}{1 - \beta u_{xc}^{\zeta-1}}. \qquad \text{(C3)}$$

For the truncated Pareto distribution of the seismic moment tensor,

$$\Phi(u) = \frac{u^{1-\zeta}-1}{u_{xp}^{1-\zeta}-1}, \quad \text{for} \quad u_{xp} > u \geq 1, \quad \text{and}$$
$$\Phi(u) = 1 \quad \text{for} \quad u \geq u_{xp}. \qquad \text{(C4)}$$

For the gamma distribution of the seismic moment,

$$\Phi(u) = \frac{P_1 - P_2}{1 - P_2}, \qquad \text{(C5)}$$

where

$$P_1 = P\left(\left(\frac{u}{u_{xg}}\right)^{d/(1-d)}, \; 1-\beta\right), \qquad \text{(C6)}$$

and

$$P_2 = P\left(\left(\frac{1}{u_{xg}}\right)^{d/(1-d)}, \; 1-\beta\right), \qquad \text{(C7)}$$

see (B7) for the definition of the P-function.

References

Abercrombie, R. E. (1995), Earthquake source scaling relationships from -1 to 5 M_L using seismograms recorded at 2.5-km depth, *J. Geophys. Res.*, *100*, 24,015-24,036.

Abramowitz, M. and Stegun, I. A. (1972), *Handbook of Mathematical Functions*, Dover, NY, pp 1046.

Aki, K. (1965), Maximum likelihood estimate of b in the formula $\log N = a - bM$ and its confidence limits, *Bull. Earthquake Res. Inst. Tokyo Univ.*, *43*, 237-239.

Anderson, J. G., and J. E. Luco (1983), Consequences of slip rate constraints on earthquake occurrence relation, *Bull. Seismol. Soc. Amer.*, *73*, 471-496.

Bebbington, M., and D. Harte (2003), The linked stress release model for spatio-temporal seismicity: formulations, procedures and applications, *Geophys. J. Int.*, *154*(3), 925-946.

Bird, P. (2003), An updated digital model of plate boundaries, *Geochemistry, Geophysics, Geosystems*, *4*(3), 1027, doi:10.1029/2001GC000252.

Bird, P., and Y. Y. Kagan (2004), Plate-tectonic analysis of shallow seismicity: apparent boundary width, beta, corner magnitude, coupled lithosphere thickness, and coupling in seven tectonic settings, *Bull. Seismol. Soc. Amer.*, *94*(6), 2390-2399.

Bodin, P., and J. N. Brune (1996), On the scaling of slip with rupture length for shallow strike-slip earthquakes – quasi-static models and dynamic rupture propagation, *Bull. Seismol. Soc. Amer.*, *86*, 1292-1299.

Brune, J. N. (1968), Seismic moment, seismicity, and rate of slip along major fault zones, *J. Geophys. Res.*, *73*, 777-784.

Chery, J., Merkel, S., and S. Bouissou (2001), A physical basis for time clustering of large earthquakes, *Bull. Seismol. Soc. Am.*, *91*, 1685-1693.

Dawson, T. E., S. F. McGill, and T. K. Rockwell (2003), Irregular recurrence of paleoearthquakes along the central Garlock fault near El Paso Peaks, California, *J. Geophys. Res.*, *108*(B7), 2356, doi:10.1029/2001JB001744.

Ebel, J. E., K.-P. Bonjer, and M. C. Oncescu (2000), Paleoseismicity: Seismicity evidence for past large earthquakes, *Seismol. Res. Lett.*, *71(2)*, 283-294.

Ekström, G., A. M. Dziewonski, N. N. Maternovskaya and M. Nettles (2003), Global seismicity of 2001: centroid-moment tensor solutions for 961 earthquakes, *Phys. Earth Planet. Inter.* *136*(3-4), 165-185.

Ellsworth, W. L. (1990), Earthquake history, 1769-1989, in: *The San Andreas fault system, California*, ed. R. E. Wallace, Geological Survey Professional Paper, P-1515, pp. 153-187.

Evans, M., N. Hastings, and B. Peacock (1993), *Statistical Distributions*, 2nd ed., New York, J. Wiley, 170 pp.

Field, E. H., D. D. Jackson, and J. F. Dolan (1999), A mutually consistent seismic-hazard source model for southern California, *Bull. Seismol. Soc. Amer.*, *89*, 559-578.

Gerstenberger, M. C., S. Wiemer, and D. Giardini (2001), A systematic test of the hypothesis that the b value varies with depth in California, *Geophys. Res. Lett.*, *28*(1), 57-60.

Hanks, T. C. (1992), Small earthquakes, tectonic forces, *Science*, *256*, 1430-1432.

Henry, C., and S. Das (2001), Aftershock zones of large shallow earthquakes: Fault dimensions, aftershock area expansion, and scaling relations, *Geophys. J. Int.*, *147*, 272-293; Erratum, *148*, p. 349.

Holt, W. E., N. Chamot-Rooke, X. Le Pichon, A. J. Haines, B. Shen-Tu, and J. Ren (2000), Velocity field in Asia inferred from Quaternary fault slip rates and Global Positioning System observations, *J. Geophys. Res.*, *105*, 19,185-19,209.

Jackson, D. D., Aki, K., Cornell, C. A., Dieterich, J. H., Henyey, T. L., Mahdyiar, M., Schwartz, D., Ward, S. N. (1995), Seismic hazards in southern California: Probable earthquakes, 1994-2024, *Bull. Seism. Soc. Am.*, *85*, 379-439.

Jackson, D. D., Shen, Z.-K., D. Potter, B.-X. Ge, and L.-Y. Sung (1997), Southern California deformation, *Science*, *277*, 1621-1622.

Jaumé, S. C., and L. R. Sykes (1996), Evolution of moderate seismicity in the San Francisco Bay region, 1850 to 1993: seismicity changes related to the occurrence of large and great earthquakes, *J. Geophys. Res.*, *101*, 765-789.

Kagan, Y. Y. (1982), Stochastic model of earthquake fault geometry, *Geophys. J. Roy. astr. Soc.*, *71*, 659-691.

Kagan, Y. Y. (1991), Fractal dimension of brittle fracture, *J. Nonlinear Sci.*, *1*, 1-16.

Kagan, Y. Y. (1996), Comment on "The Gutenberg-Richter or characteristic earthquake distribution, which is it?" by S. G. Wesnousky, *Bull. Seismol. Soc. Amer.*, *86*, 274-285.

Kagan, Y. Y. (1999), Universality of the seismic moment-frequency relation, *Pure Appl. Geoph.*, *155*, 537-573.

Kagan, Y. Y. (2002a), Seismic moment distribution revisited: I. Statistical results,

Kagan, Y. Y. (2002b), Seismic moment distribution revisited: II. Moment conservation principle,

Kagan, Y. Y. (2002c), Aftershock zone scaling, *Bull. Seismol. Soc. Amer.*, *92*, 641-655.

Kagan, Y. Y., and D. D. Jackson (1991), Long-term earthquake clustering, *Geophys. J. Int.*, *104*, 117-133.

Kagan, Y. Y. and D. D. Jackson (1999), Worldwide doublets of large shallow earthquakes, *Bull. Seismol. Soc. Amer.*, *89*, 1147-1155.

Kagan, Y. Y., and D. D. Jackson (2000), Probabilistic forecasting of earthquakes, *Geophys. J. Int.*, *143*, 438-453.

Kagan, Y. Y., D. D. Jackson, and Z. Liu (2005), Stress and earthquakes in southern California, 1850-2004, JGR, this issue, accepted; http://scec.ess.ucla.edu/~ykagan/cstress_index.html .

Kagan, Y. Y., and L. Knopoff (1980), Spatial distribution of earthquakes: The two-point correlation function, *Geophys. J. Roy. astr. Soc.*, *62*, 303-320.

King, G. (1983), The accommodation of large strains in the upper lithosphere of the Earth and other solids by self-similar fault systems: the geometrical origin of b-value, *Pure Appl. Geophys.*, *121*, 761-815.

King, G., D. Oppenheimer, and F. Amelung (1994), Block versus continuum deformation in the Western United States, *Earth Planet. Sci. Lett.*, *128*, 55-64.

Kreemer, C., W. E. Holt, and A. J. Haines (2003), An integrated global model of present-day plate motions and plate boundary deformation, *Geophys. J. Int.*, *154*, 8-34, doi:10.1046/j.1365-246X.2003.01917.x

Leonard, T., O. Papsouliotis, and I. G. Main (2001), A Poisson model for identifying characteristic size effects in frequency data: Application to frequency-size distributions for global earthquakes, 'starquakes' and fault lengths, *J. Geophys. Res.*, *106*, 13,473-13,484.

Libicki, E., and Y. Ben-Zion (2005), Stochastic branching models of fault surfaces and estimated fractal dimension, *Pure Appl. Geoph.*, accepted.

Liu, J., Y. Klinger, K. Sieh and C. Rubin (2004), Six similar sequential ruptures of the San Andreas fault, Carrizo Plain, California, *Geology*, *32*(8), 649-652, doi: 10.1130/G20478.1.

Mai, P. M., and G. C. Beroza (2002), A spatial random field model to characterize complexity in earthquake slip, *J. Geophys. Res.*, *107*(B11), Art. No. 2308.

Main, I. (2000), Apparent breaks in scaling in the earthquake cumulative frequency-magnitude distribution: fact or artifact?, *Bull. Seismol. Soc. Amer.*, *90*, 86-97.

Mori, J., and R. E. Abercrombie (1997), Depth dependence of earthquake frequency-magnitude distributions in California: implications for rupture initiation, *J. Geophys. Res.*, *102*, 15081-90.

Natawidjaja, D. H., K. Sieh, S. N. Ward, H. Cheng, R. L. Edwards, J. Galetzka, and B. W. Suwargadi (2004), Paleogeodetic records of seismic and aseismic subduction from central Sumatran microatolls, Indonesia, *J. Geophys. Res.*, *109*(B4), Art. No. B04306.

Okal, E. A., and B. A. Romanowicz (1994), On the variation of b-values with earthquake size, *Phys. Earth Planet. Inter.*, *87*, 55-76.

Pacheco, J. F., C. H. Scholz, and L. R. Sykes (1992), Changes in frequency-size relationship from small to large earthquakes, *Nature*, *355*, 71-73.

Pérez, O. J., and C. H. Scholz (1997), Long-term seismic behavior of the focal and adjacent regions of great earthquakes during the time between two successive shocks, *J. Geophys. Res.*, *102*, 8203-8216.

Reid, H. F. (1910), Elastic rebound theory, *Univ. Calif. Publ. Bull. Dept. Geol. Sci.*, *6*, 92-120.

Rockwell, T. K., Lindvall, S., Herzberg, M., Murbach, D., Dawson, T., and G. Berger (2000), Paleoseismology of the Johnson Valley, Kickapoo, and Homestead Valley faults: clustering of earthquakes in the eastern California shear zone, *Bull. Seismol. Soc. Amer.*, *90*, 1200-1236.

Rockwell, T. K., S. Lindvall, T. Dawson, R. Langridge, W. Lettis, and Y. Klinger (2002), Lateral offsets on surveyed cultural features resulting from the 1999 Izmit and Duzce earthquakes, Turkey *Bull. Seismol. Soc. Amer.*, *92*(1), 79-94.

Romanowicz, B. (1994), A reappraisal of large earthquake scaling – comment, *Bull. Seismol. Soc. Amer.*, *84*, 1675-1676.

Romanowicz, B., and L. J. Ruff, 2002. On moment-length scaling of large strike slip earthquakes and the strength of faults, *Geophys. Res. Lett.*, **29**(12), Art. No. 1604, doi:10.1029/2001GL014479.

Rong, Y.-F., D. D. Jackson and Y. Y. Kagan (2003), Seismic gaps and earthquakes, *J. Geophys. Res.*, *108*(B10), 2471, *ESE-6*, pp. 1-14, doi:10.1029/2002JB002334.

Rundle, J. B. (1989), Derivation of the complete Gutenberg-Richter magnitude-frequency relation using the principle of scale invariance, *J. Geophys. Res.*, *94*, 12,337-12,342.

Sagiya, T. (2004), A decade of GEONET: 1994-2003 - The continuous GPS observation in Japan and its impact on earthquake studies, *Earth Planet. Space*, *56*(8), XXIX-XLI.

Scholz, C. H. (1997), Size distributions for large and small earthquakes, *Bull. Seismol. Soc. Amer.*, *87*, 1074-1077.

Scholz, C. H. (1998), A further note on earthquake size distributions, *Bull. Seismol. Soc. Amer.*, *88*, 1325-1326.

Scholz, C. H. (2002), *The Mechanics of Earthquakes and Faulting*, Cambr. Univ. Press, Cambridge, 2nd ed., pp. 471.

Scharer, K. M., R. J. Weldon, T. E. Fumal, and G. P. Biasi (2003), Paleoseismic data used to evaluate long term earthquake behavior, *Eos Trans. AGU*, *84*(46), Fall AGU Meet. Suppl., (abstract), T51A-03.

Schwartz, D. P., and K. J. Coppersmith (1984), Fault behavior and characteristic earthquakes: Examples from Wasatch and San Andreas fault zones, *J. Geophys. Res., 89,* 5681-5698.

Shearer, P., E. Hauksson, G. Lin and D. Kilb (2003), Comprehensive waveform cross-correlation of southern California seismograms: Part 2. Event locations obtained using cluster analysis, *Eos Trans. AGU*, *84*(46), Fall Meet. Suppl., Abstract S21D-0326.

Shimazaki, K., and T. Nakata (1980), Time-predictable recurrence model for large earthquakes, *Geophys. Res. Lett.*, *7*, 279-282.

Sieh, K., M. Stuiver, and D. Brillinger (1989), A more precise chronology of earthquakes produced by the San Andreas fault in Southern California, *J. Geophys. Res.*, *94*, 603-623.

Sornette, D., L. Knopoff, Y. Y. Kagan, and C. Vanneste (1996), Rank-ordering statistics of extreme events: Application to the distribution of large earthquakes, *J. Geophys. Res.*, *101*, 13,883-13,893.

Stein, S., and A. Newman (2004), Characteristic and uncharacteristic earthquakes as possible artifacts: Application to the New Madrid and Wabash seismic zones, *Seismol. Res. Lett.*, *75*(2), 173-187.

Stock, C., and E. G. C. Smith (2000), Evidence for different scaling of earthquake source parameters for large earthquakes depending on faulting mechanism, *Geophys. J. Int.*, *143*, 157-162.

Toppozada, T., D. Branum, M. Petersen, C. Hallstrom, C. Cramer, and M. Reichle (2000), *Epicenters of and Areas Damaged by $M \geq 5$ California Earthquakes, 1800-1999*, Map sheet 49, Div. Mines Geology, California.

Triep, E. G., and L. R. Sykes (1997), Frequency of occurrence of moderate to great earthquakes in intracontinental regions: Implications for changes in stress, earthquake prediction, and hazards assessments, *J. Geophys. Res.*, *102*, 9923-9948.

Utsu, T. (1999), Representation and analysis of the earthquake size distribution: A historical review and some new approaches, *Pure Appl. Geophys.*, *155*, 509-535.

Utsu, T., Y. Ogata, and R. S. Matsu'ura (1995), The centenary of the Omori formula for a decay law of aftershock activity, *J. Phys. Earth*, *43*, 1-33.

Vere-Jones, D. (1976), A branching model for crack propagation, *Pure Appl. Geophys.*, *114*, 711-725.

Ward, S. N. (2004), Earthquake simulation by restricted random walks, *Bull. Seismol. Soc. Amer.*, *94*(6), 2079-2089.

Weldon, R. J., T. E. Fumal, T. J. Powers, S. K. Pezzopane, K. M. Scharer, and J. C. Hamilton (2002), Structure and earthquake offsets on the San Andreas fault at the Wrightwood, California, paleoseismic site, *Bull. Seismol. Soc. Amer.*, *92*, 2704-2725.

Wells, D. L., and K. J. Coppersmith (1994), New empirical relationships among magnitude, rupture length, rupture width, rupture area, and surface displacement, *Bull. Seismol. Soc. Amer.*, *84*, 974-1002.

Wesnousky, S. G. (1986), Earthquakes, Quaternary faults, and seismic hazard in California, *J. Geophys. Res.*, *91*, 12,587-12,631.

Wesnousky, S. G. (1994), The Gutenberg-Richter or characteristic earthquake distribution, Which is it?, *Bull. Seismol. Soc. Amer.*, *84*, 1940-1959.

Wesnousky, S. G. (1996), The Gutenberg-Richter or characteristic earthquake distribution, which is it? Reply, *Bull. Seismol. Soc. Amer.*, *86*(1), 286-291.

Wyss, M., C. G. Sammis, R. M. Nadeau, and S. Wiemer (2004), Fractal dimension and *b*-value on creeping and locked patches of the San Andreas fault near Parkfield, California, *Bull. Seismol. Soc. Amer.*, *94*, 410-421.

Wolfram, S. (1999), *The Mathematica Book*, 4th ed., Cambridge University Press, pp. 1470.

Yeats, R. S., K. Sieh, and C. R. Allen (1997), *The Geology of Earthquakes*, New York, Oxford Univ. Press, 568 pp.

Zaliapin, I. V., Y. Y. Kagan, and F. Schoenberg (2005), Approximating the distribution of Pareto sums, *Pure Appl. Geoph.*, accepted; http://scec.ess.ucla.edu/~ykagan/zks_index.html .

Zheng, X. G., and D. Vere-Jones (1994), Further applications of the stochastic stress release model to historical earthquake data, *Tectonophysics*, *229*, 101-121.

Yan Y. Kagan, Department of Earth and Space Sciences, University of California, Los Angeles, California, 90095-1567, USA; (e-mail: ykagan@ucla.edu)

Table 1. Values of exponents for the scale-invariant part of various fault geometrical distributions

		$L \propto M^{1/d}$			$u \propto M^{(d-1)/d}$		$u \propto M^{1/3}$ $(d = 3)$				
d	M	M_s	L	L_s	u	u_s	u	u_s	u_p	u'	u'_s
1	2	3	4	5	6	7	8	9	10	11	12
	β	ξ		κ			ζ				
		$\frac{\beta d-1}{d}$	βd	$\beta d-1$	$\frac{\beta d}{d-1}$	$\frac{\beta d-1}{d-1}$	βd	$\beta d-1$	$\beta d-2$	$\frac{\beta d}{d-1}$	$\frac{\beta d-1}{d-1}$
1.5	2/3	0	1	0	2	0	–	–	–	–	–
2.0	2/3	1/6	4/3	1/3	4/3	1/3	–	–	–	–	–
3.0	2/3	1/3	2	1	1	1/2	2	1	0	1	1/2
3.0	0.6	4/15	1.8	0.8	0.9	0.4	1.8	0.8	−0.2	0.9	0.4
3.0	1/2	1/6	3/2	1/2	3/4	1/4	3/2	1/2	−1/2	3/4	1/4

[a] x – area-specific distributions;
[b] x_s – site-specific distributions;
[c] x_p – point-specific distributions;
[d] x'_s – reduced site-specific slip for small earthquakes, $m \leq 7$.
Columns 3-7, 11-12 assume rupture width $W \leq W_0$ (15 km);
Columns 8-10 width W is not limited, $d = 3$ scaling is assumed;

β – area-specific moment distribution exponent;
ξ – site-specific moment distribution exponent;
κ – site-specific rupture length distribution exponent;
ζ – site-specific slip distribution exponent.

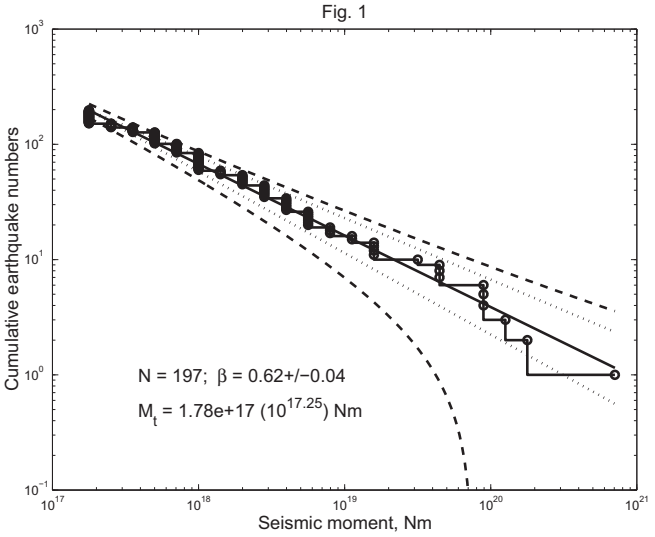

Figure 1. Number of earthquakes (shown by circles) with seismic moment larger than or equal to M as a function of M for the earthquakes in the *Toppozada et al.* [2000] catalog. Latitude limits 32.5°N – 37.0°N, magnitude threshold 5.5, the total number of events is 197. Solid line – is the fit to these assuming a Pareto distribution (3) with the exponent $\beta = 0.621 \pm 0.044$; dotted lines show 95% confidence limits [*Aki*, 1965]. Dashed lines are uncertainties in earthquake numbers when assuming a Poisson distribution of the numbers and using the Gaussian approximation for the Poisson distribution.

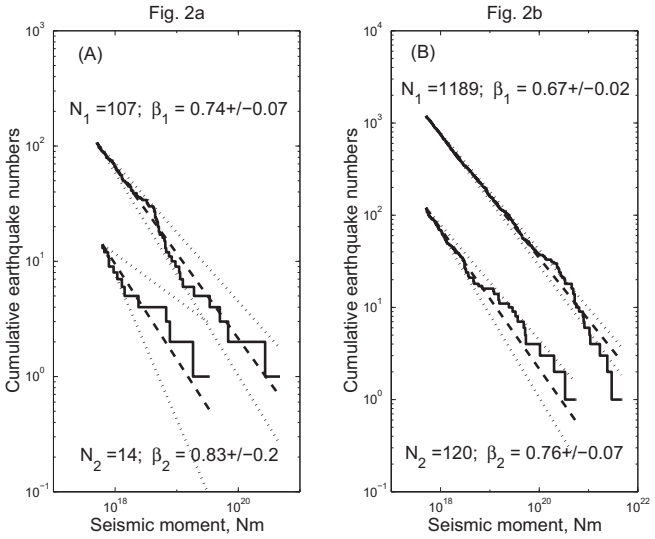

Figure 2. Seismic moment statistical distribution, Harvard catalog 1977/1/1 – 2002/09/30 [*Ekström et al.*, 2003], subduction zones. Moment threshold is $10^{17.7}$ Nm ($m \geq 5.8$). Upper four curves – earthquakes on ocean side; lower curves – earthquakes on continental side. Solid line – approximation by a Pareto distribution (3), dashed lines 95% confidence limits [*Aki*, 1965], conditioned by the total number of earthquakes observed. The limits show approximately the uncertainty due to the β-value estimation error. The number of events should follow the Poisson distribution with these parameter values; hence the full uncertainties would be higher. For smaller time intervals the Poisson distribution is far from the Gaussian, the accurate formula is given by *Kagan* [1996, Eq. 16]. The total number of earthquakes N and the exponent β estimate is shown for both populations.
(A) – strike-slip earthquakes;
(B) – thrust earthquakes.

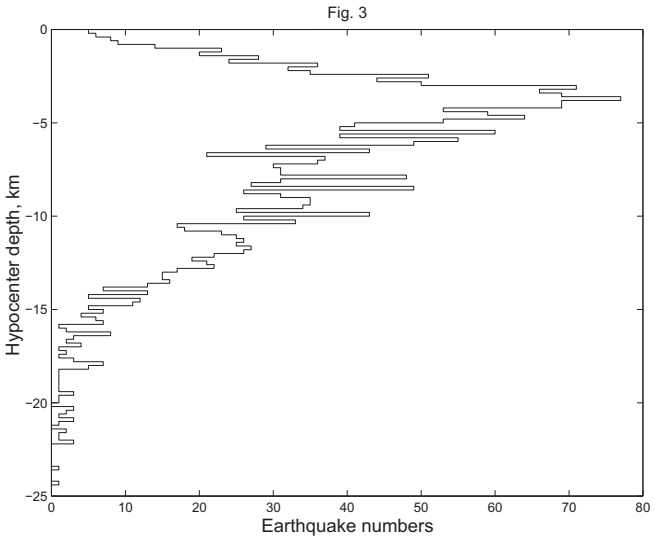

Figure 3. Depth histogram for hypocenters estimated using a waveform cross-correlation technique in the 1992-1994 southern California catalog of *Shearer et al.* [2003]. A magnitude threshold $M_L \geq 3.0$ is used. The number of earthquakes is 2547, the average depth $\bar{h} = 6.9$ km, the standard deviation $\sigma_h = 4.1$ km.

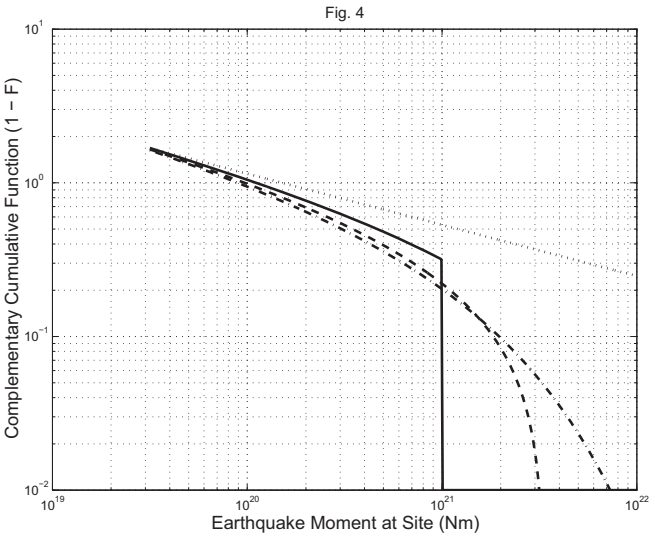

Figure 4. Probability functions for the site-specific moment distribution for $M \propto L^{3.0}$. Solid line – truncated G-R cumulative distribution – model (a) in Section 3.1; dashed line – truncated G-R distribution density (b); dash-dotted line – modified gamma distribution (d). Dotted line corresponds to the unrestricted G-R distribution.

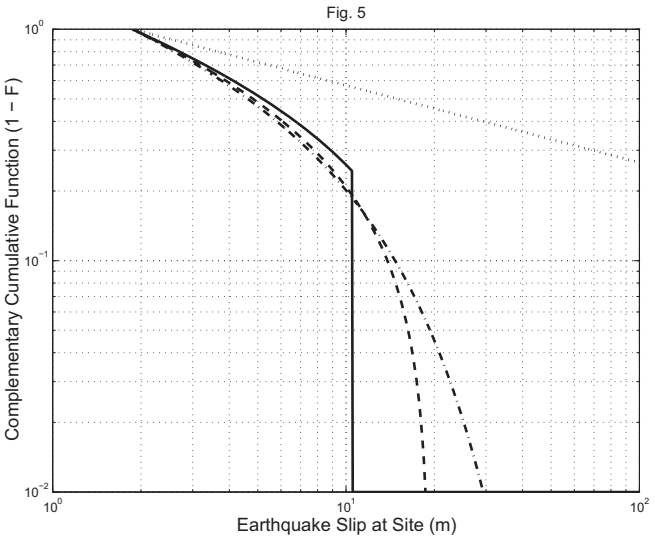

Figure 5. Probability functions for the site-specific slip distribution in individual earthquakes for $M \propto L^{2.0}$. Solid line – truncated G-R cumulative distribution – model (a) in Section 3.1; dashed line – truncated G-R distribution density (b); dash-dotted line – modified gamma distribution (d). Dotted line corresponds to the asymptotic distribution $u_x \to \infty$, i.e., $\Psi(u) = u^{-\zeta}$ (see Equation (A4)).

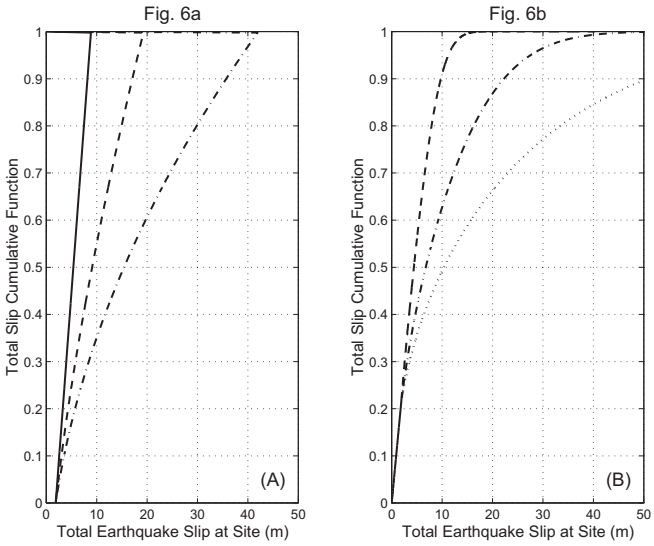

Figure 6. Cumulative probability functions for total earthquake slip distribution at a single site. Solid line – $M \propto L^{3.0}$ for small earthquakes ($m \leq 7$); dashed line – $M \propto L^{1.5}$; dash-dotted line – $M \propto L^{2.0}$; dotted line – $M \propto L^{3.0}$.
(A) the truncated G-R distribution density – model (b) in Section 3.1.
(B) the gamma distribution density – model (d) in Section 3.1.

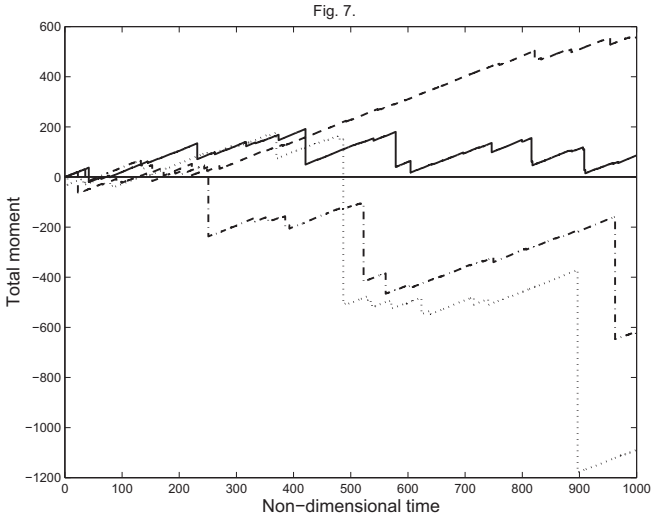

Figure 7. Simulations of the seismic moment release history. Four examples are shown. Each represents an independent simulation of moment release history. Earthquakes are assumed to occur according to the Poisson law; the moment distribution is assumed to be the truncated power-law distribution density (5) with $\beta = 2/3$. For illustration we use the maximum moment equal to 1000 and the minimum size earthquake is equal to 1.0. If the moment unit is assumed to equal 10^{18} Nm, the maximum magnitude (or the maximum jump in the diagram) corresponds to an $m8$ earthquake.

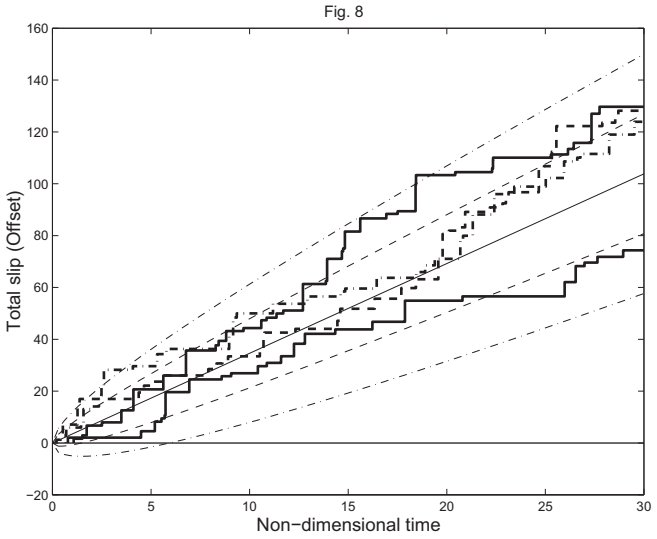

Figure 8. Simulation of slip trajectory versus time at a arbitrary site (thick lines, solid and dot-dashed), Poisson in time, truncated Pareto in slip ($\zeta = 1/3$, $u_{xp} = 10.33$ m). Dashed thin lines – Gaussian approximation (see Equations 30, 31) for the sum, $\pm\sigma$. Dash-dotted thin lines – Gaussian approximation for the sum, $\pm 2\sigma$.

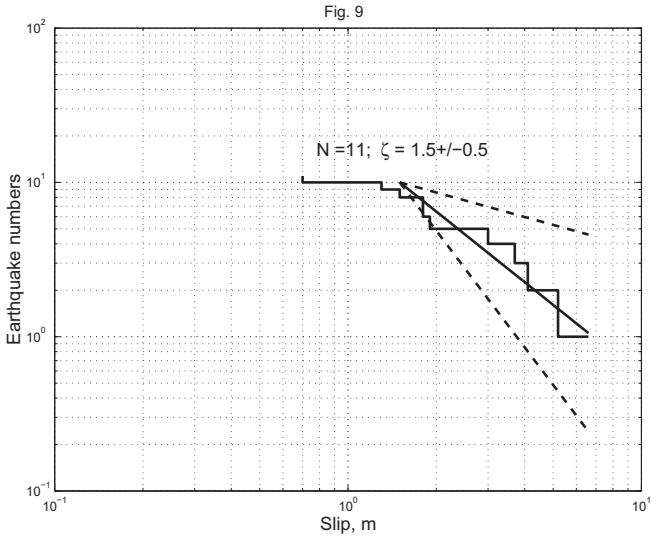

Figure 9. Slip statistical distribution, for paleoseismic measurements made in the San Andreas at Wrightwood, CA. Threshold (minimum) slip is 1.5 m. Solid line – approximation by a power-law Pareto distribution, $\zeta = 1.52 \pm 0.51$; dashed lines 95% confidence limits [*Aki*, 1965], conditioned by the total number of earthquakes observed.

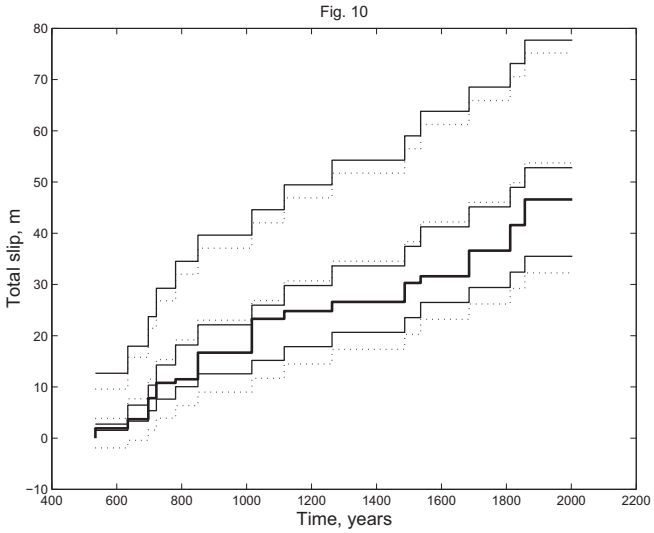

Figure 10. Slip trajectory versus time, San Andreas at Wrightwood, CA; thick solid line – measurements, thin solid lines – simulations, thin dotted lines – Gaussian approximations [see Equations (30) and (31)]. Average estimate (middle thin lines) and 95% confidence limits (upper and lower thin lines) are shown.